Chemical genetic approaches for target validation

Wel, T. van der

6

A natural substrate activity assay for high-throughput screening on monoacylglycerol lipase

Introduction

Lipid metabolism is a tightly regulated cellular process involving enzymes responsible for spatiotemporal lipid biosynthesis and degradation. Homeostasis of lipids is often dysregulated in disease, for example in (auto-)immune disorders and cancer.[1–3] Monoacylglycerol lipase (MAGL) is a membrane-associated serine hydrolase responsible for breakdown of monoacylglycerols into free fatty acids (FFAs) and glycerol. The enzyme employs a serine-histidine-aspartate catalytic triad to cleave the ester bond of monoacylglycerols, whereas it is unable to hydrolyze di- or triacylglycerols.[4,5] Structurally, MAGL possesses a typical α/β hydrolase fold, composed of a central β-sheet flanked on both sides by eight α-helices.[6] Access to the active site is probably regulated by a hydrophobic lid domain that allows the enzyme to adopt either an open or closed conformational state.[7] The open conformation presumably allows association to the membrane and recruitment of its substrate, after which the lid domain closes and MAGL dissociates.[8]

MAGL was initially discovered as the main enzyme responsible for degradation of the endocannabinoid 2-arachidonoylglycerol (2-AG) in the brain (Figure 6.1).[9] The signaling lipid 2-AG is an endogenous ligand of the cannabinoid (CB) 1 and 2 receptors, which are involved in various physiological processes, such as appetite, pain, emotion and energy homeostasis.[10] Hydrolysis of 2-AG by MAGL terminates CB receptor activation and

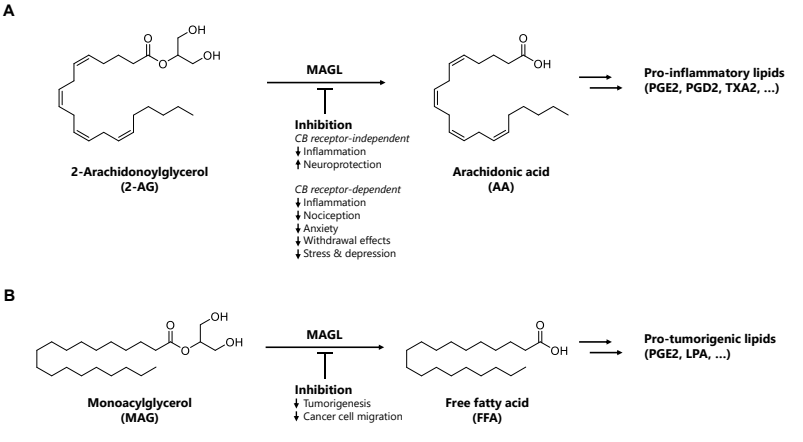

Figure 6.1 – Monoacylglycerol lipase is a central player in biosynthesis of free fatty acids from monoacylglycerols. **(A)** MAGL is the main enzyme responsible for degradation of 2-arachidonoylglycerol (2-AG) into arachidonic acid (AA) in the brain. Inhibition of MAGL results in neuroprotection and reduced inflammation due to lowered cellular pools of AA, which is a precursor for pro-inflammatory lipids such as prostaglandins E2/D2 (PGE2/PGD2) and thromboxane A2 (TXA2). In addition, MAGL inhibition prolongs 2-AG-mediated CB receptor signaling, resulting in various CB receptor-dependent physiological effects. **(B)** Free fatty acids (FFAs) produced by hydrolysis of monoacylglycerols (MAGs) by MAGL are precursors for pro-tumorigenic lipids such as PGE2 and lysophosphatidic acid (LPA). Inhibition of MAGL results in lower cellular FFA pools and reduces tumorigenesis and cancer cell migration.

liberates free arachidonic acid (AA). In turn, AA is a precursor of pro-inflammatory eicosanoids such as prostaglandins.[3,11]

More recently, MAGL was found to also be highly expressed in various aggressive human cancer cells and primary tumors in comparison with nonaggressive counterparts.[12] MAGL probably contributes to the cancer pathogenesis via multiple mechanisms by directly increasing *de novo* synthesis of FFAs, making tumor cells less dependent on lipid uptake from the extracellular environment.[2,13] FFAs are required for the biosynthesis of cell membranes and pro-tumorigenic signaling molecules, such as lysophosphatidic acid (LPA) and prostaglandin E2 (PGE2).[12,14] In addition, FFAs can be used as a direct energy source, for example by beta-oxidation in the mitochondrial matrix to generate ATP.[15]

The central role of MAGL in lipid metabolism makes it a potential therapeutic target for a variety of disorders. Recently, the irreversible MAGL inhibitor ABX-1431, developed by Abide Therapeutics, has shown promising data in Phase 1 clinical studies in patients with Tourette syndrome.[16,17] In addition, pharmacological inhibition of MAGL showed beneficial effects in various inflammation-related disease models, such as amyotrophic lateral sclerosis (ALS)[18], multiple sclerosis (MS)[19] and Parkinson's and Alzheimer's disease.[20] MAGL inactivation also exerts CB1R-dependent anti-nociceptive effects[21], reduces anxiety[22], attenuates withdrawal symptoms in drug addiction[23] and ameliorates stress and depression in mouse models.[24] Finally, inhibition of MAGL reduced cancer cell migration, invasion and survival[25], and slowed tumor growth.[12,26]

Most reported MAGL inhibitors have an irreversible mode of action, forming a covalent complex after nucleophilic attack by the catalytic serine. As therapeutics, irreversible inhibitors can have several benefits, such as increased potency and a long residence time that can drive pharmacological efficacy. Furthermore, irreversible binders may have an advantageous pharmacodynamics profile, since no excessive circulating levels of inhibitor are required to maintain target engagement.[27] On the other hand, the irreversible mode of action may also have several drawbacks. Idiosyncratic drug-related toxicity remains a point of concern, either by formation of reactive drug metabolites with poorly predictable effects or by haptenization of covalent inhibitor-enzyme adducts that may trigger an immune response.[28,29] In case of MAGL inhibition specifically, chronic exposure to irreversible inhibitor JZL184 resulted in pharmacological tolerance, development of physical dependence, impaired synaptic plasticity and receptor desensitization in the nervous system.[30,31]

The question thus rises whether inhibition of MAGL by reversible binders may avoid these undesirable side-effects. However, most described MAGL inhibitors have an irreversible mode of action and compounds that target MAGL in a reversible manner are currently underrepresented.[19,32] In addition, most compounds lack potency, selectivity or

the right physicochemical properties for use in *in vivo* studies. Therefore, it is of great relevance to identify novel chemotypes to reversibly inhibit MAGL.

Here, the optimization and miniaturization of a biochemical activity assay for MAGL is described, which was subsequently applied in a high-throughput screen on 233,820 unique compounds within the Cancer Drug Discovery Initiative (CDDI). Hit validation was performed using an orthogonal gel-based activity-based protein profiling assay, ultimately resulting in qualified hits that constitute starting points for the development of novel, reversible MAGL inhibitors.

Results

Assay setup and optimization

Although widely used in high-throughput screening assays for their ease of detection, surrogate substrates generally have an attenuated binding affinity for the enzyme active site compared to physiologically relevant natural substrates. This may lead to distorted results when determining inhibitor potency. For this reason, a MAGL activity assay was set up and optimized employing its natural substrate 2-AG.[33] Glycerol production from 2-AG by MAGL is coupled to the generation of a fluorescent signal using an enzymatic cascade reaction (Figure 6.2A).[5] The continuous assay setup and fluorescence readout in multi-well plates ensures HTS compatibility.

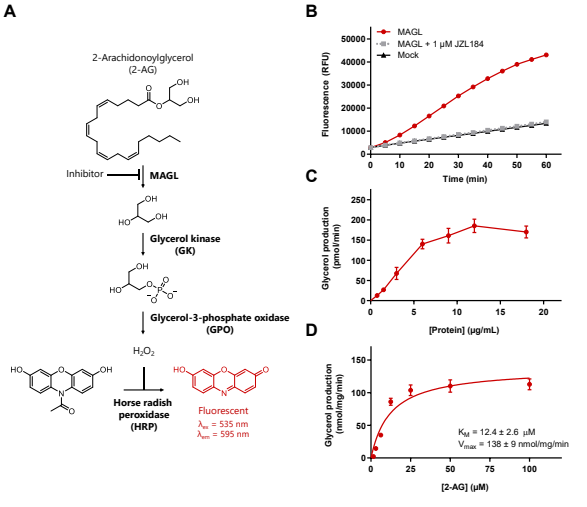

Figure 6.2 – MAGL activity assay setup and optimization in 96-well plate format. (A) Hydrolysis of 2-AG by MAGL is linked to the production of a fluorescent signal via an enzymatic cascade reaction. Liberated glycerol is phosphorylated by glycerol kinase (GK), followed by oxidation to dihydroxyacetone phosphate and hydrogen peroxide using glycerol-3-phosphate oxidase (GPO). The produced hydrogen peroxide is used by horse radish peroxidase (HRP) to oxidize Amplifu™Red to fluorescent resorufin. **(B)** Time course of 2-AG hydrolysis by MAGL, as measured by resorufin fluorescence. **(C, D)** Glycerol production by MAGL as function of protein (C) or substrate (D) concentration. Data shown are means ± SEM (N = 2, n = 2).

First, full-length human MAGL was transiently overexpressed in HEK293T cells, after which membrane fractions were isolated. Cells transfected with empty vector (mock) served as a control for background fluorescence from 2-AG hydrolysis by endogenous hydrolases in these cells. Membranes were incubated with assay mix containing 2-AG and components required for the enzymatic cascade reaction. Assays were initially performed in 96-well plates in a total volume of 200 µL. A time-dependent increase in fluorescence was observed, which was reduced to mock-levels upon pre-incubation with MAGL inhibitor JZL184 (Figure 6.2B). The measured glycerol production rates were dependent on the used protein concentration, with a linear range up to 10 µg/mL (Figure 6.2C). In a similar fashion, reaction rates were measured at various concentrations of 2-AG (Figure 6.2D), resulting in a V_{max} of 138 ± 9 nmol/mg/min and an apparent K_M of 12 ± 3 µM, which is in line with a previous report using the same assay setup.[34]

Next, the assay was miniaturized to 384-well format in a reaction volume of 30 µL. Using a two-fold increase in protein concentration (from 1.5 to 3 ng/µL in 96- to 384-well format, respectively), similar reaction progression curves were observed as in 96-well format (Figure 6.3A). Under these assay conditions, MAGL activity is dose-dependently inhibited by MAGL inhibitor JZL184 with a pIC_{50} of 7.6 ± 0.05 (Figure 6.3B), which is in the same nanomolar range as previously reported.[35] Assay conditions were sufficiently robust for further miniaturization, as reflected by decent Z'-factors (> 0.6) and S/B ratios (> 5). Intra-assay variability was assessed by measuring the reaction rates of 64 individual positive and negative control samples in a single plate, resulting in a coefficient of variation of 6.6% and 7.5% respectively.

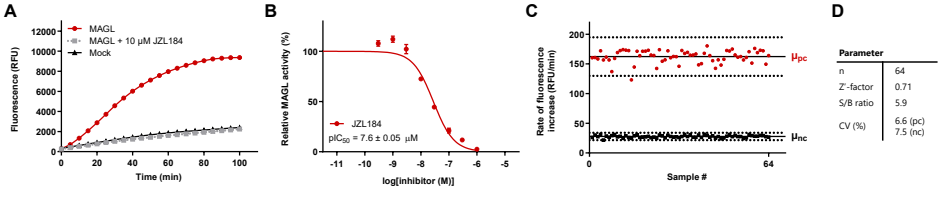

Figure 6.3 – Miniaturization of MAGL activity assay to 384-well plate format. (A) Time course of 2-AG hydrolysis by MAGL, as measured by resorufin fluorescence. **(B)** Dose-response curve of MAGL inhibitor JZL184. **(C)** Intra-assay variability plot. Solid lines represent the mean of individual data points (μ_{pc}/μ_{nc}); dashed lines represent µ ± 3σ. **(D)** Assay performance parameters. S/B: signal to background; CV: coefficient of variation. Data shown are means ± SEM (n = 64 for A-C; N = 2, n = 2 for B).

Within the Cancer Drug Discovery Initiative, the assay was then further miniaturized to 1536-well format. The assay reaction volume was further reduced to 4 µL and protein concentrations were increased to 9 ng/µL to improve the S/B ratio. In addition, the assay buffer was supplemented with 0.03% (w/w) Tween-20 to improve assay performance. End point instead of kinetic measurements were performed to simplify the data analysis process. Validation runs demonstrated that the assay was sufficiently reproducible and robust for use in a HTS campaign.

High-throughput screening

In total, 233,820 compounds were screened in the optimized 1536-well assay, divided over two days. Assays were performed at a single dose of 10 µM inhibitor with 30 min pre-incubation. Screening quality was assessed by calculating the Z'-factor (Figure 6.4A) and S/B ratio (Figure 6.4B) for each of the 188 individual plates. Plates measured on day 2 showed better overall performance than those measured on day 1, but all plates met the requirement of Z'-factor >0.6. All screened compounds were categorized by percentage MAGL inhibition (Figure 6.4C) and the 1,555 compounds showing ≥ 50% inhibition at 10 µM were designated as primary assay hits, corresponding to a hit rate of 0.67% (Table 6.1). Using a nearest neighbor clustering model, potential false negatives were added to the hit list, resulting in a number of 4,389 compounds. Active confirmation was then performed on these compounds using the exact same assay conditions, resulting in a list of confirmed actives of 1,142 compounds. Subsequently, a deselection assay was performed using glycerol instead of 2-AG as the substrate. This deselection assay aims to exclude false positives, for example compounds that interfere with the assay setup. This is particularly relevant in case of an enzymatic cascade assay, since inhibition of either of the enzymes downstream of MAGL will result in a reduced fluorescent signal. After deselection, the remaining 334 compounds were further reduced to 146 compounds by applying a more stringent criterion of >60% inhibition at 10 µM in the primary assay. Subsequently, structures were examined and compounds with an apparent irreversible mode of action were excluded at this stage, as well as those with poor physicochemical properties or protection by intellectual property. This triage process resulted in a qualified hit list of 50 compounds of which chemical structures were disclosed.

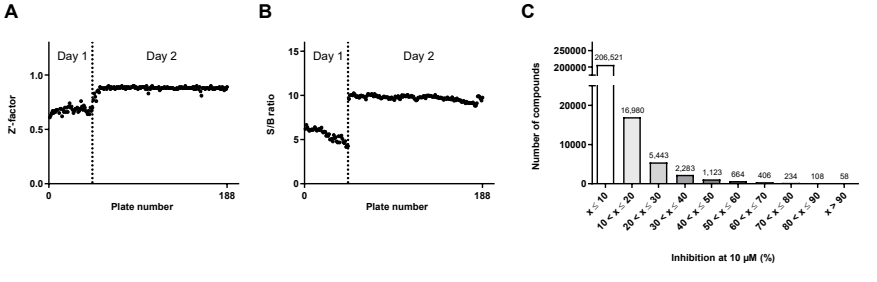

Figure 6.4 – High throughput screen overview of assay quality and hits. (A, B) Screen quality assessed by Z'-factor (A) and S/B ratio (B) for each individual 1536-well plate. Plates 1-46 were measured on day 1, plates 47-188 on day 2. **(C)** Overview of screened compounds categorized by percentage MAGL inhibition at 10 µM.

Table 6.1 – High-throughput screen triage process. Criteria and cut-offs used at each step are indicated. DRC: dose-response curve, ABPP: activity-based protein profiling.

	Remaining compounds	Criterion	% of total
Complete screen	233,820	-	100%
Primary assay hits	1,555	≥ 50% inhibition at 10 µM	0.67%
Nearest neighbors	4,389	Clustering algorithm; < 50% inhibition at 10 µM	1.88%
Active confirmation	1,142	≥ 50% inhibition at 10 µM in confirmation assay	0.49%
Deselection	334	< 10% inhibition on glycerol conversion at 10 µM	0.14%
Stringency	146	> 60% inhibition at 10 µM	0.06%
Triage	111	Chemical eye, mode of action, intellectual property	0.05%
DRC	50	IC_{50}, no time dependence	0.02%
Orthogonal assay	7	> 25% inhibition at 10 µM in ABPP assay	0.003%

Within the qualified hit list, 9 clusters of different chemotypes could be distinguished (Table 6.2), many of which contained piperidine or piperazine structural motifs. Of note, the clusters of benzoxazine derivatives **1**-**6** and piperazine amide **34** were already previously reported as MAGL inhibitors.[36] Many identified clusters, such as benzoxazine derivatives **1**-**6**, imidazopiperidines **13**-**16**, naphtyl amides **20**-**28**, phenyl thiazoles **29**-**30** and piperidine amides **31**-**33**, all possess favorable physicochemical properties (MW <500 g/mol, cLogP <5).[37] Other clusters, however, such as the (fused) imidazopyridines **9**-**12** and **17**-**19** have higher cLogP values and therefore overall lower LipEs. The tPSA of nearly all compounds is <90 $Å^2$, which is the generally accepted upper limit for molecules to cross the blood-brain barrier, except for carbamate **7**, singletons **35** and **40** and sulfonamides **47** and **48**. All qualified hits were measured in dose-response experiments and pIC_{50} values were determined at various time points. No clear time-dependent inhibition, indicative of an irreversible mode of action, was observed for any of the compounds. The hit pIC_{50} values ranged from 4.7 to 6.9 (Table 6.2).

Table 6.2 – Qualified hit list. Hits are clustered by chemotype. Purity (> 90%) and mass were confirmed by LC-MS. Deviations from expected mass are shown as ΔMW. pIC_{50} values were determined in end point measurement after 45 min. Percentages inhibition in orthogonal ABPP assay are relative to vehicle-treated controls. Physicochemical properties (cLogP, tPSA, HBD, HBA) were calculated using ChemDraw Professional 16.0. MW: molecular weight; tPSA: topological polar surface area; HBD: number of hydrogen bond donors; HBA: number of hydrogen bond acceptors; LipE: lipophilic efficiency (LipE = pIC_{50} primary assay – cLogP); LE: ligand efficiency (LE = 1.4 x pIC_{50}/N where N = number of non-hydrogen atoms). [+] A mass discrepancy of 16 Da that may indicate an under-oxidized analog of the intended compound.

Cluster	Entry	Structure	MW (Da)	Confirmed purity	Confirmed mass	ΔMW (Da)	pIC_{50} primary assay	Inhibition ABPP assay (%)	cLogP	tPSA (Å^2)	HBD	HBA	LipE	LE
Benzoxazine derivative	**1**	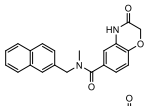	346	Yes	Yes	-	5.5	-3	3.16	58.6	1	3	2.3	0.29
Benzoxazine derivative	**2**	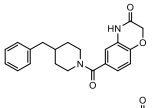	350	No	Yes	-	6.8	-2	2.92	58.6	1	3	3.8	0.36
Benzoxazine derivative	**3**	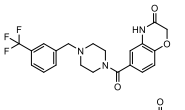	419	Yes	Yes	-	6.5	17	3.13	61.9	1	7	3.3	0.30
Benzoxazine derivative	**4**	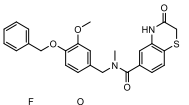	449	Yes	Yes	-	6.1	13	3.86	67.9	1	4	2.2	0.27
Benzoxazine derivative	**5**	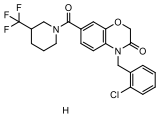	453	Yes	Yes	-	6.0	-6	3.56	49.9	0	6	2.4	0.27
Benzoxazine derivative	**6**	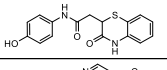	314	Yes	Yes	-	5.6	2	1.58	78.4	3	3	4.0	0.36
Carbamate	**7**	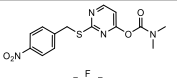	334	Yes	Yes	-	5.4	-4	2.12	106.1	0	4	3.3	0.33
Carbamate	**8**	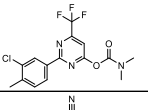	360	Yes	Yes	-	5.8	2	3.83	54.3	0	6	2.0	0.34
Fused imidazopyridine	**9**	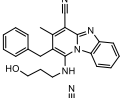	370	No	Yes	-	6.0	-13	5.16	71.7	2	5	0.9	0.30
Fused imidazopyridine	**10**	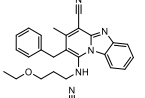	399	Yes	Yes	-	6.2	2	6.30	60.7	1	5	-0.1	0.30
Fused imidazopyridine	**11**	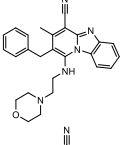	426	Yes	Yes	-	6.3	-11	5.77	63.9	1	6	0.6	0.28
Fused imidazopyridine	**12**	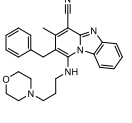	440	Yes	Yes	-	6.0	-12	6.04	63.9	1	6	0.0	0.26

Table 6.2 – Qualified hit list (continued).

Cluster	Entry	Structure	MW (Da)	Confirmed purity	Confirmed mass	ΔMW (Da)	pIC_{50} primary assay	Inhibition ABPP assay (%)	cLogP	tPSA ($Å^2$)	HBD	HBA	LipE	LE
Imidazopiperidine	**13**	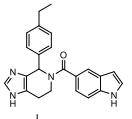	370	Yes	No†	+371	5.5	10	3.56	56.7	2	4	2.0	0.29
Imidazopiperidine	**14**	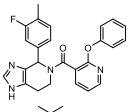	428	Yes	Yes	-	5.7	17	3.88	66.3	1	6	1.8	0.25
Imidazopiperidine	**15**	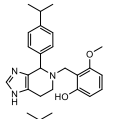	377	Yes	Yes	-	5.8	9	4.00	57.1	2	5	1.8	0.29
Imidazopiperidine	**16**	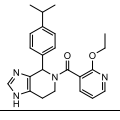	390	Yes	Yes	-	6.3	6	3.87	66.3	1	5	2.4	0.30
Imidazopyridines	**17**	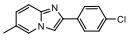	243	Yes	Yes	-	5.4	-10	4.72	15.6	0	2	0.7	0.45
Imidazopyridines	**18**	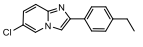	257	Yes	Yes	-	5.4	4	5.26	15.6	0	2	0.1	0.42
Imidazopyridines	**19**	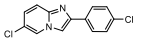	263	Yes	Yes	-	5.6	10	4.94	15.6	0	2	0.7	0.46
Naphtyl amide	**20**	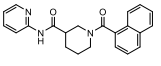	359	No	No	+113	5.7	-9	3.14	61.8	1	3	2.5	0.29
Naphtyl amide	**21**	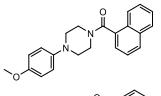	346	Yes	No	+28	5.8	51	3.96	32.8	0	3	1.8	0.31
Naphtyl amide	**22**	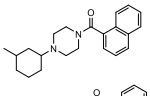	336	No	Yes	-	6.2	16	4.97	23.6	0	2	1.3	0.35
Naphtyl amide	**23**	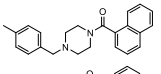	344	No	No	+45	4.9	-4	4.73	23.6	0	2	0.2	0.26
Naphtyl amide	**24**	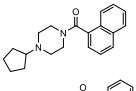	308	No	Yes	-	5.5	-11	3.77	23.6	0	2	1.7	0.35
Naphtyl amide	**25**	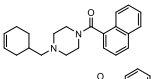	334	Yes	Yes	-	5.3	-7	4.55	23.6	0	2	0.7	0.30
Naphtyl amide	**26**	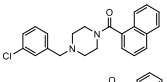	365	Yes	Yes	-	5.4	24	4.94	23.6	0	2	0.5	0.29
Naphtyl amide	**27**	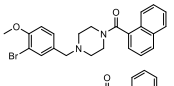	439	Yes	Yes	-	6.2	-17	4.92	32.8	0	3	1.3	0.31
Naphtyl amide	**28**	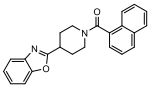	356	Yes	Yes	-	5.7	69	3.42	41.9	0	3	2.3	0.30

Table 6.2 – Qualified hit list (continued).

Cluster	Entry	Structure	MW (Da)	Confirmed purity	Confirmed mass	ΔMW (Da)	pIC_{50} primary assay	Inhibition ABPP assay (%)	cLogP	tPSA (Å^2)	HBD	HBA	LipE	LE
Phenyl thiazole	**29**	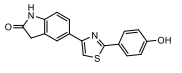	308	Yes	Yes	-	5.8	1	2.96	61.7	2	3	2.9	0.37
Phenyl thiazole	**30**	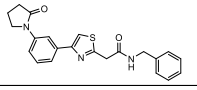	391	Yes	No	+15	5.9	11	3.12	61.8	1	3	2.8	0.30
Piperidine amide	**31**	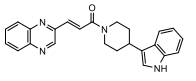	382	No	Yes	-	5.6	49	3.43	57.1	1	4	2.2	0.27
Piperidine amide	**32**	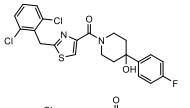	465	Yes	Yes	-	5.6	16	3.93	52.9	1	4	1.7	0.26
Piperidine amide	**33**	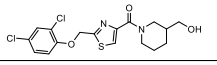	401	Yes	Yes	-	5.8	5	2.13	62.1	1	4	3.7	0.33
Singleton	**34**	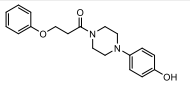	326	No	Yes	-	5.6	-1	2.97	53.0	1	4	2.6	0.33
Singleton	**35**	To be disclosed	490	Yes	No	-16†	6.2	86	3.09	135.8	0	6	3.1	0.26
Singleton	**36**	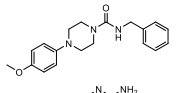	325	Yes	Yes	-	5.5	-6	3.39	44.8	1	3	2.1	0.32
Singleton	**37**	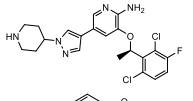	450	Yes	Yes	-	5.5	18	4.29	75.2	2	7	1.2	0.26
Singleton	**38**	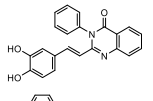	356	Yes	Yes	-	5.5	12	4.08	73.1	2	4	1.5	0.29
Singleton	**39**	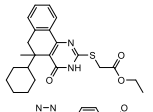	413	Yes	Yes	-	4.7	-3	5.59	67.8	1	3	-0.9	0.23
Singleton	**40**	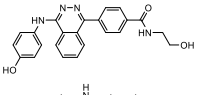	400	No	Yes	-	5.7	2	3.18	106.3	4	6	2.5	0.26
Singleton	**41**	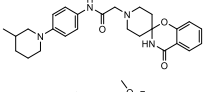	449	Yes	Yes	-	6.0	6	3.29	73.9	2	5	2.7	0.25
Singleton	**42**	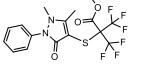	428	No	Yes	-	5.5	7	2.94	49.9	0	9	2.6	0.28
Singleton	**43**		155	Yes	No	+205	5.7	0	-1.12	51.2	0	4	6.8	0.80

Table 6.2 – Qualified hit list (continued).

Cluster	Entry	Structure	MW (Da)	Confirmed purity	Confirmed mass	ΔMW (Da)	pIC_{50} primary assay	Inhibition ABPP assay (%)	cLogP	tPSA (Å^2)	HBD	HBA	LipE	LE
Singleton	**44**	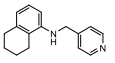	238	Yes	Yes	-	6.0	62	3.16	24.4	1	2	2.9	0.47
Singleton	**45**	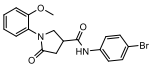	389	Yes	Yes	-	5.9	46	4.32	58.6	1	3	1.6	0.34
Sulfonamide	**46**	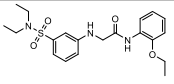	406	Yes	Yes	-	5.5	18	3.20	87.7	2	5	2.3	0.27
Sulfonamide	**47**	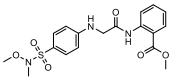	407	No	Yes	-	6.1	-7	1.94	114.0	2	6	4.2	0.31
Sulfonamide	**48**	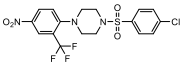	450	No	No	+22	6.3	13	5.08	92.4	0	7	1.2	0.30
Sulfonamide	**49**	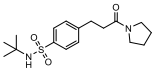	338	Yes	Yes	-	6.9	32	1.54	66.5	1	3	5.3	0.42
Sulfonamide	**50**	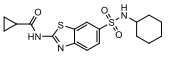	379	No	No	+328	5.5	0	4.20	87.6	2	4	1.3	0.31

Hit validation by orthogonal ABPP assay

Next, the qualified hits were tested in an orthogonal gel-based competitive activity-based protein profiling (ABPP) assay on mouse brain membrane proteome. The used probe, FP-TAMRA, is a broad-spectrum probe that targets a wide range of serine hydrolases including the endocannabinoid hydrolases MAGL, fatty acid amide hydrolase (FAAH) and alpha/beta hydrolase domain-containing protein 6 (ABHD6). Remarkably, in an initial competitive ABPP assay using standard labeling conditions (500 nM FP-TAMRA, 15 min incubation), no significant inhibition was observed for any of the compounds (data not shown). This is probably due to the irreversible mode of action of probe FP-TAMRA, resulting in rapid outcompetition of reversible inhibitors. This was addressed by reducing probe concentration and incubation time (100 nM FP-TAMRA, 10 min incubation), resulting in 7 compounds showing >25% inhibition at 10 µM under these conditions (Figure 6.5A, 6.5C, Table 6.2, Supplementary Figure 6.1). Interestingly, some chemotypes (benzoxazine derivatives **1**-**6** and naphtyl amides **20**-**28**) showed decent inhibition in the primary assay but were ineffective in the ABPP assay. A correlation between inhibitor potency in the primary substrate-based assay and orthogonal ABPP assay was observed for all compounds except **49**, which was the most potent hit in the primary assay but showed poorest inhibition in the ABPP assay (Figure 6.5B). At this point, compound purity and mass were analyzed by LC-MS, which revealed that 14 of the 50 qualified hits were <90% pure and 9 compounds differed in mass. Of note, the most potent inhibitor identified by ABPP

(compound **35**) showed a mass discrepancy of 16 Da, which might indicate that this may be an under-oxidized analog of the intended compound.

Competitive ABPP is a powerful technique to obtain an initial selectivity profile of the qualified hits. Most tested compounds showed good selectivity profiles on the mouse brain membrane proteome at 10 µM (Figure 6.5A). However, 7 compounds showed >25% inhibition of FAAH, the endocannabinoid hydrolase responsible for degradation of the endocannabinoid anandamide (Figure 6.5D). Direct comparison of MAGL versus FAAH labeling profiles (Figure 6.5E) revealed that compound **35** is the most potent MAGL inhibitor and selective over FAAH at 10 µM, making it an interesting candidate for further hit optimization.

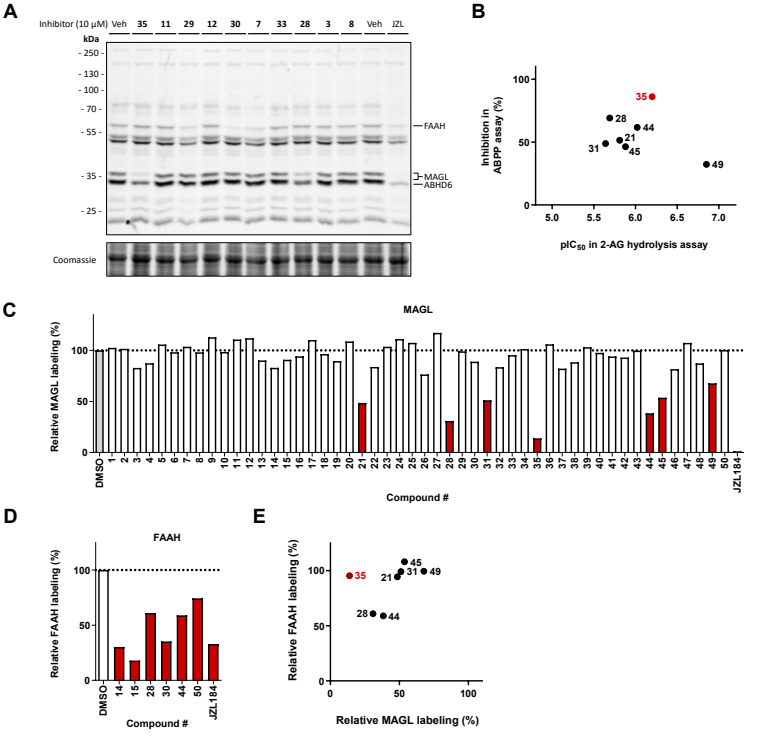

Figure 6.5 – Hit validation and selectivity assessment in orthogonal activity-based protein profiling (ABPP) assay. **(A)** Competitive ABPP assay on mouse brain membrane proteome using FP-TAMRA. Proteome was pre-incubated with inhibitor (10 µM, 30 min), followed by incubation with FP-TAMRA (100 nM, 10 min). JZL184 was included as positive control. **(B)** Correlation between primary 2-AG hydrolysis activity assay and orthogonal competitive ABPP assay. **(C, D)** Quantification of MAGL (C) and FAAH (D) band intensity as described in A, corrected for relative protein loading determined by Coomassie staining (N = 1). **(E)** Correlation between MAGL and FAAH inhibition determined by competitive ABPP.

Conclusion

A 2-AG hydrolysis assay for MAGL was successfully optimized and miniaturized to 1536-well format. Subsequently, this assay was applied in a high-throughput screen on 233,820 compounds. This resulted in a total of 1,142 confirmed hits, which after deselection and hit triage resulted in a qualified hit list of 50 compounds that were measured in dose-response assays. In total 10 clusters of different chemotypes could be identified, among which two were previously reported as MAGL inhibitors. Many of these clusters have favorable physicochemical properties, such as low MW, cLogP and tPSA. The 50 qualified hits were analyzed in an orthogonal gel-based competitive ABPP assay. Although reversible inhibition was challenging to detect using the irreversibly binding probe FP-TAMRA, 7 compounds showed >25% inhibition of MAGL. Comparison of labeling profiles in the mouse brain proteome revealed the qualified hit selectivity profiles, with FAAH being a prominent off-target of several compounds. Altogether, given its inhibitory potency, favorable selectivity profile and good physicochemical properties, compound **35** may be an especially interesting candidate for further hit optimization efforts.

Acknowledgments

Tsang-Wai Lam and Helma Rutjes are kindly acknowledged for their contributions to the miniaturization and optimization of the assay for the high-throughput screen, Hui Deng for collaboration with hit validation experiments and Constant A.A. van Boeckel for the hit triage process.

Experimental procedures

General

All chemicals, oligonucleotides and other reagents were purchased from Sigma Aldrich, unless stated otherwise. Oligo sequences can be found in Supplementary Table 6.1. Cloning reagents and FP-TAMRA probe were purchased at Thermo Fisher Scientific. Assay enzymes (glycerol kinase from *Cellulomonas sp.,* product code G6142; glycerol-3-phosphate oxidase from *Streptococcus thermophilus*, product code G4388; horse radish peroxidase from *Horseradish,* product code 77332) were purchased from Sigma Aldrich. 2-Arachidonoylglycerol was purchased from Cayman Chemicals. High-throughput screen was performed at Pivot Park Screening Centre (Oss, The Netherlands) and executed within the Cancer Drug Discovery Initiative.

Cloning

Full-length cDNA encoding human MAGL (Source Bioscience) was amplified by PCR and cloned into expression vector pcDNA3.1 in frame with a C-terminal FLAG-tag. All plasmids were isolated from transformed XL10-Gold competent cells (prepared using *E. coli* transformation buffer set; Zymo Research) using plasmid isolation kits following the supplier's protocol (Qiagen). Constructs were verified by Sanger sequencing (Macrogen).

Supplementary Table 6.1 – List of oligonucleotide sequences.

ID	Name	Sequence
P1	MAGL_forw	CTTAAGCTTTGGTACCGCCGCCACCATGGAAACAGGACCTGAAG
P2	MAGL_rev	CATTCTAGATCACTCGAGACCGGTGGGTGGGGACGCAGTTC

Cell culture

HEK293T (human embryonic kidney) cells were obtained from ATCC and tested on regular basis for mycoplasma contamination. Cultures were discarded after 2-3 months of use. Cells were cultured at 37 °C under 7% CO2 in DMEM containing phenol red, stable glutamine, 10% (v/v) high iron newborn calf serum (Seradigm), penicillin and streptomycin (200 µg/mL each; Duchefa). Medium was refreshed every 2-3 days and cells were passaged two times a week at 80-90% confluence. One day prior to transfection, HEK293T cells were transferred from confluent 10 cm dishes to 15 cm dishes (16 dishes for HTS). Before transfection, medium was refreshed (13 mL). A 3:1 mixture of polyethyleneimine (PEI; 60 µg/dish) and plasmid DNA (20 µg/dish) was prepared in serum-free medium (2 mL) and incubated for 15 min at rt. The mixture was then dropwisely added to the cells, after which the cells were grown to confluence in 72 h. Cells were then harvested by suspension in PBS, followed by centrifugation (200 *g*, 5 min). Cell pellets were flash-frozen in liquid nitrogen and stored at -80 °C until membrane fraction preparation.

Membrane fraction preparation

Mouse brains were isolated according to guidelines approved by the ethical committee of Leiden University (DEC#13191), frozen in liquid nitrogen and stored at -80 °C until use. Cell pellets or mouse brains were thawed on ice and homogenized by polytron (20,000 rpm, 3 x 7 s; SilentCrusher S, Heidolph) in lysis buffer A (20 mM HEPES pH 7.2, 2 mM DTT, 250 mM sucrose, 1 mM $MgCl_2$ and 25 U/mL benzonase). Suspensions were incubated on ice for 30 min, followed by low speed centrifugation (2500 *g*, 3 min, 4 °C) to remove debris. Supernatants were then subjected to ultracentrifugation (93,000 *g,* 30 min, 4 °C; Beckman Coulter, Ti70 or Ti70.1 rotor). Pellets were homogenized in storage buffer B (20 mM HEPES pH 7.2, 2 mM DTT) by polytron (20,000 rpm, 1 x 10 s). Protein concentrations were determined using Quick Start™ Bradford Protein Assay (Bio-Rad). Membrane preparations were frozen in liquid nitrogen and stored at -80 °C until use.

Biochemical MAGL activity assays and deselection assay

96-well format

Assays were performed in HEMNB buffer (50 mM HEPES pH 7.4, 1 mM EDTA, 5 mM $MgCl_2$, 100 mM NaCl, 0.5% (w/w) BSA) in black, flat-bottom 96-well plates (Greiner). Inhibitors were added from 40x concentrated stock solution in DMSO. MAGL-overexpressing membrane preparations (0.3 µg per well) were incubated with inhibitor for 20 min at rt in a total volume of 100 µL. Next, 100 µL assay mix containing glycerol kinase (GK), glycerol-3-phosphate oxidase (GPO), horse radish peroxidase (HRP), adenosine triphosphate (ATP), Amplifu™Red and 2-arachidonoylglycerol (2-AG) was added. Fluorescence (λ_{ex} = 535 nm, λ_{em} = 595 nm) was measured at rt in 5 min intervals for 60 min on a GENios plate reader (Tecan). Final assay concentrations: 1.5 ng/µL MAGL-overexpressing membranes, 0.2 U/mL GK, GPO and HRP, 125 µM ATP, 10 µM Amplifu™Red, 25 µM 2-AG, 5% DMSO, 0.5% ACN in a total volume of 200 µL. All measurements were performed in N = 2 (individual plates), n = 2 (technical replicates on same plate) or N = 2, n = 4 for controls, with $Z' \geq 0.6$. For K_M and IC_{50} determinations, the assay was performed as described above, but with variable 2-AG and inhibitor concentrations, respectively.

384-well format

Assays were performed as described for the 96-well format, unless stated otherwise. Assays were performed in black, flat-bottom 384-well plates (Greiner). Inhibitors (40x concentrated stock solution in DMSO) and MAGL-overexpressing membranes were diluted in HEMNB buffer to 2x concentrated solutions. Membranes (10 µL) were incubated with inhibitor (10 µL) for 20 min at rt, after which assay mix (10 µL of 3x concentrated solution) was added. Final assay concentrations were same as in 96-well format, but with 3 ng/µL MAGL-overexpressing membranes in a total volume of 30 µL. Fluorescence (λ_{ex} = 535 nm, λ_{em} = 595 nm) was measured at rt in 5 min intervals for 100 min on an Infinite M1000 Pro plate reader (Tecan).

1536-well format

Assays were performed as described for the 96-well format, unless stated otherwise. Assays were performed in black, flat-bottom non-treated 1536-well plates (Corning 3724). HEMNB buffer was supplemented with 0.03% (w/w) Tween-20. Inhibitors (200x concentrated stock solution in DMSO, 20 nL per well) were added using acoustic dispensing (Labcyte 555 Echo Liquid Handler) and diluted in assay buffer (1 µL). Membranes (2 µL) were added and mixtures were incubated for 30 min at rt, after which assay mix (1 µL) was added. Final assay concentrations were same as in 96-well format, but with 9 ng/µL MAGL-overexpressing membranes in a total volume of 4 µL. Fluorescence (λ_{ex} = 531 nm, λ_{em} = 595 nm) end point measurement was performed after 45 min incubation at rt on an EnVision Multimode plate reader (Perkin Elmer). Deselection assays were performed as described for the 1536-well format MAGL assay, but with glycerol (12.5 µM) instead of 2-AG as substrate.

Activity-based protein profiling

Inhibitor solutions (50 nL in DMSO, final concentration 10 µM) were added to 384-well plates using acoustic dispensing (Labcyte 555 Echo Liquid Handler), after which mouse brain membrane preparation (10 µL, 2 mg/mL) was added. The mixture was incubated for 30 min at rt, followed by incubation with FP-TAMRA (0.5 µL in DMSO, final concentration 100 nM, 10 min, rt). Reactions were quenched with 4x Laemmli buffer (3.5 µL, final concentrations 60 mM Tris pH 6.8, 2% (w/v) SDS, 10% (v/v) glycerol, 5% (v/v) β-mercaptoethanol, 0.01% (v/v) bromophenol blue) for 30 min at rt. Samples (18 µg protein) were resolved by SDS-PAGE on a 10% polyacrylamide gel (180 V, 75 min). Gels were scanned using Cy3 channel settings (605/50 filter; ChemiDoc™ MP System, Bio-Rad). Fluorescence intensity was corrected for protein loading determined by Coomassie Brilliant Blue R-250 staining and quantified with Image Lab (Bio-Rad).

Data analysis and statistics

Fluorescence values were corrected for the average fluorescence of the negative control (mock-membranes + vehicle for 96- and 384-well format, MAGL-overexpressing membranes + 10 µM JZL184 for 1536-well format). MAGL-overexpressing membranes incubated with vehicle served as a positive control. Slopes of the corrected data were determined in the linear interval. If relevant, the slopes in RFU/min were converted into slopes in nmol converted glycerol per milligram protein per minute via a glycerol standard curve with the rate of fluorescence increase as a function of converted glycerol. The Z′-factor for each assay plate was calculated using the formula $Z' = 1 - 3(\sigma_{pc} + \sigma_{nc})/(\mu_{pc} - \mu_{nc})$ with σ = standard deviation, µ = mean, pc = positive control and nc = negative control. Plates with $Z' \geq 0.6$ were accepted for further analysis. For K_M and V_{max} determination, data were subjected to Michaelis-Menten analysis (GraphPad Prism 5.0). For IC_{50} determination, slopes were normalized to the positive control and analyzed in a non-linear dose-response analysis with variable slope (GraphPad Prism 5.0). All shown data represent means ± SEM, unless stated otherwise.

Supplementary Data

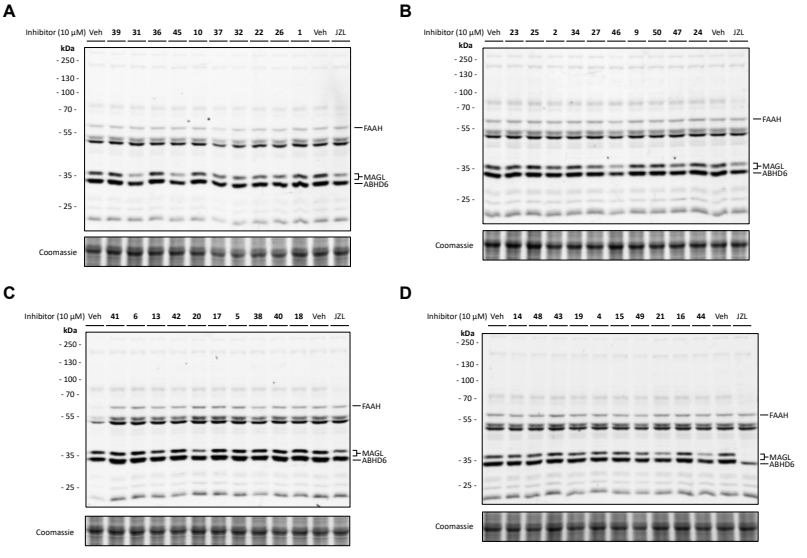

Supplementary Figure 6.1 – Complete set of activity-based protein profiling (ABPP) assays. Competitive ABPP assay on mouse brain membrane proteome using FP-TAMRA. Proteome was pre-incubated with inhibitor (10 µM, 30 min), followed by incubation with FP-TAMRA (100 nM, 10 min). JZL184 was included as positive control on all gels. Quantification of MAGL and FAAH labeling intensity can be found in Figure 6.5.

References

1. Buckley, M. L. & Ramji, D. P. The influence of dysfunctional signaling and lipid homeostasis in mediating the inflammatory responses during atherosclerosis. *Biochimica et Biophysica Acta - Molecular Basis of Disease* **1852**, 1498–1510 (2015).
2. Currie, E., Schulze, A., Zechner, R., Walther, T. C. & Farese, R. V. Cellular fatty acid metabolism and cancer. *Cell Metabolism* **18**, 153–161 (2013).
3. Serhan, C. N., Chiang, N. & Van Dyke, T. E. Resolving inflammation: Dual anti-inflammatory and pro-resolution lipid mediators. *Nature Reviews Immunology* **8**, 349–361 (2008).
4. Bertrand, T. *et al.* Structural Basis for Human Monoglyceride Lipase Inhibition. *J. Mol. Biol.* **396**, 663–673 (2010).
5. Navia-Paldanius, D., Savinainen, J. R. & Laitinen, J. T. Biochemical and pharmacological characterization of human α/β-hydrolase domain containing 6 (ABHD6) and 12 (ABHD12). *J. Lipid Res.* **53**, 2413–2424 (2012).
6. Schalk-Hihi, C. *et al.* Crystal structure of a soluble form of human monoglyceride lipase in complex with an inhibitor at 1.35 A ° resolution. *Protein Sci.* **20**, 670–683 (2011).
7. Labar, G. *et al.* Crystal structure of the human monoacylglycerol lipase, a key actor in endocannabinoid signaling. *ChemBioChem* **11**, 218–227 (2010).
8. Riccardi, L. *et al.* Lid domain plasticity and lipid flexibility modulate enzyme specificity in human monoacylglycerol lipase. *Biochim. Biophys. Acta - Mol. Cell Biol. Lipids* **1862**, 441–451 (2017).
9. Blankman, J. L., Simon, G. M. & Cravatt, B. F. A Comprehensive Profile of Brain Enzymes that Hydrolyze the Endocannabinoid 2-Arachidonoylglycerol. *Chem. Biol.* **14**, 1347–1356 (2007).
10. Blankman, J. L. & Cravatt, B. F. Chemical probes of endocannabinoid metabolism. *Pharmacol. Rev.* **65**, 849–71 (2013).
11. Mulvihill, M. M. & Nomura, D. K. Therapeutic potential of monoacylglycerol lipase inhibitors. *Life Sci.* **92**, 492–497 (2013).
12. Nomura, D. K. *et al.* Monoacylglycerol Lipase Regulates a Fatty Acid Network that Promotes Cancer Pathogenesis. *Cell* **140**, 49–61 (2010).
13. Omabe, M., Ezeani, M. & Omabe, K. N. Lipid metabolism and cancer progression: The missing target in metastatic cancer treatment. *Journal of Applied Biomedicine* **13**, 47–59 (2015).
14. Zaidi, N. *et al.* Lipogenesis and lipolysis: The pathways exploited by the cancer cells to acquire fatty acids. *Progress in Lipid Research* **52**, 585–589 (2013).
15. DeBerardinis, R. J., Lum, J. J., Hatzivassiliou, G. & Thompson, C. B. The Biology of Cancer: Metabolic Reprogramming Fuels Cell Growth and Proliferation. *Cell Metabolism* **7**, 11–20 (2008).
16. Cisar, J. S. *et al.* Identification of ABX-1431, a Selective Inhibitor of Monoacylglycerol Lipase and Clinical Candidate for Treatment of Neurological Disorders. *J. Med. Chem.* **61**, 9062–9084 (2018).
17. Jiang, M. & Van Der Stelt, M. Activity-Based Protein Profiling Delivers Selective Drug Candidate ABX-1431, a Monoacylglycerol Lipase Inhibitor, to Control Lipid Metabolism in Neurological Disorders. *Journal of Medicinal Chemistry* **61**, 9059–9061 (2018).
18. Pasquarelli, N. *et al.* Evaluation of monoacylglycerol lipase as a therapeutic target in a transgenic mouse model of ALS. *Neuropharmacology* **124**, 157–169 (2017).
19. Hernández-Torres, G. *et al.* A reversible and selective inhibitor of monoacylglycerol lipase ameliorates multiple sclerosis. *Angew. Chemie - Int. Ed.* **53**, 13765–13770 (2014).
20. Chen, R. *et al.* Monoacylglycerol Lipase Is a Therapeutic Target for Alzheimer's Disease. *Cell Rep.* **2**, 1329–1339 (2012).
21. Griebel, G. *et al.* Selective blockade of the hydrolysis of the endocannabinoid 2-arachidonoylglycerol impairs learning and memory performance while producing antinociceptive activity in rodents. *Sci. Rep.* **5**, 7642 (2015).
22. Kinsey, S. G., O'Neal, S. T., Long, J. Z., Cravatt, B. F. & Lichtman, A. H. Inhibition of endocannabinoid catabolic enzymes elicits anxiolytic-like effects in the marble burying assay. *Pharmacol. Biochem. Behav.* **98**, 21–27 (2011).
23. Ramesh, D. *et al.* Dual inhibition of endocannabinoid catabolic enzymes produces enhanced antiwithdrawal effects in morphine-dependent mice. *Neuropsychopharmacology* **38**, 1039–1049 (2013).
24. Zhong, P. *et al.* Monoacylglycerol lipase inhibition blocks chronic stress-induced depressive-like behaviors via activation of mTOR signaling. *Neuropsychopharmacology* **39**, 1763–1776 (2014).
25. Nomura, D. K. *et al.* Monoacylglycerol lipase exerts dual control over endocannabinoid and fatty acid pathways to support prostate cancer. *Chem. Biol.* **18**, 846–856 (2011).
26. Pagano, E. *et al.* Pharmacological inhibition of MAGL attenuates experimental colon carcinogenesis. *Pharmacol. Res.* **119**, 227–236 (2017).
27. Barf, T. & Kaptein, A. Irreversible protein kinase inhibitors: Balancing the benefits and risks. *J. Med. Chem.* **55**, 6243–6262 (2012).
28. Singh, J., Petter, R. C., Baillie, T. A. & Whitty, A. The resurgence of covalent drugs. *Nature Reviews Drug*

Discovery **10**, 307–317 (2011).
29. King, A. R. *et al.* Discovery of Potent and Reversible Monoacylglycerol Lipase Inhibitors. *Chem. Biol.* **16**, 1045–1052 (2009).
30. Schlosburg, J. E. *et al.* Chronic monoacylglycerol lipase blockade causes functional antagonism of the endocannabinoid system. *Nat. Neurosci.* **13**, 1113–1119 (2010).
31. Chanda, P. K. *et al.* Monoacylglycerol Lipase Activity Is a Critical Modulator of the Tone and Integrity of the Endocannabinoid System. *Mol. Pharmacol.* **78**, 996–1003 (2010).
32. Tuccinardi, T. *et al.* Identification and characterization of a new reversible MAGL inhibitor. *Bioorganic Med. Chem.* **22**, 3285–3291 (2014).
33. van der Wel, T. *et al.* A natural substrate-based fluorescence assay for inhibitor screening on diacylglycerol lipase α. *J. Lipid Res.* **56**, 927–935 (2015).
34. Savinainen, J. R. *et al.* Robust Hydrolysis of Prostaglandin Glycerol Esters by Human Monoacylglycerol Lipase (MAGL). *Mol. Pharmacol.* **86**, 522–535 (2014).
35. Long, J. Z. *et al.* Selective blockade of 2-arachidonoylglycerol hydrolysis produces cannabinoid behavioral effects. *Nat. Chem. Biol.* **5**, 37–44 (2009).
36. Granchi, C., Caligiuri, I., Minutolo, F., Rizzolio, F. & Tuccinardi, T. A patent review of Monoacylglycerol Lipase (MAGL) inhibitors (2013-2017). *Expert Opinion on Therapeutic Patents* **27**, 1341–1351 (2017).
37. Hitchcock, S. A. & Pennington, L. D. Structure-brain exposure relationships. *Journal of Medicinal Chemistry* **49**, 7559–7583 (2006).